TSpace Research Repository tspace.library.utoronto.ca

Colloidal Quantum Dot Photovoltaics Enhanced by Perovskite Shelling

Zhenyu Yang, Alyf Janmohamed, Xinzheng Lan, F. Pelayo Garcia de Arquer, Oleksandr Voznyy, Emre Yassitepe, Gi-Hwan Kim, Zhijun Ning, Xiwen Gong, Riccardo Comin, and Edward H. Sargent

Version Post-Print/Accepted Manuscript

Citation (published version) Yang, Z., Janmohamed, A., Lan, X., García de Arquer, F. P., Voznyy, O., Yassitepe, E., Kim, G.-H., Ning, Z., Gong, X., Comin, R., and Sargent, E. H. (2015). Colloidal quantum dot Photovoltaics enhanced by Perovskite shelling. *Nano Letters*, *15*(11), 7539–7543. doi:10.1021/acs.nanolett.5b03271

Publisher's Statement This document is the Accepted Manuscript version of a Published Work that appeared in final form in *Nano Letters*, copyright ©American Chemical Society after peer review and technical editing by the publisher. To access the final edited and published work see http://dx.doi.org/10.1021/acs.nanolett.5b03271.

How to cite TSpace items

Always cite the published version, so the author(s) will receive recognition through services that track citation counts, e.g. Scopus. If you need to cite the page number of the TSpace version (original manuscript or accepted manuscript) because you cannot access the published version, then cite the TSpace version **in addition to** the published version using the permanent URI (handle) found on the record page.

UNIVERSITY OF TORONTO LIBRARIES

Colloidal Quantum Dot Photovoltaics Enhanced by Perovskite Shelling

Zhenyu Yang,[†,§] Alyf Janmohamed,[†,§] Xinzheng Lan,[†] F. Pelayo García de Arquer,[†] Oleksandr Voznyy,[†] Emre Yassitepe,[†] Gi-Hwan Kim,[†] Zhijun Ning,[†,¶] Xiwen Gong,[†] Riccardo Comin,[†] and Edward H. Sargent[,†]*

[†] The Edward S. Rogers Department of Electrical and Computer Engineering, University of Toronto, 10 King's College Road, Toronto, Ontario M5S 3G4, Canada

[§] Indicates equal contribution

[¶] School of Physical Science and Technology, ShanghaiTech University, 100 Haike Rd., Pudong New Area, Shanghai, 201210, China

ABSTRACT

Solution-processed quantum dots are a promising material for large-scale, low-cost solar cell applications. New device architectures and improved passivation have been instrumental in increasing the performance of quantum dot photovoltaic devices. Here we report photovoltaic devices based on inks of quantum dot on which we grow thin perovskite shells in solid-state films. Passivation using the perovskite was achieved using a facile solution ligand exchange followed by post-annealing. The resulting hybrid nanostructure created a more intrinsic CQD film, which, when incorporated into a photovoltaic device with graded bandstructure, achieved a record solar cell performance for single-step-deposited CQD films, exhibiting an AM1.5 solar power conversion efficiency of 8.95%.

KEYWORDS: Colloidal quantum dots, solar cells, perovskites, ligand exchange, surface passivation

Colloidal quantum dots (CQDs) show promise as solar harvesting materials in view of their size-tunable bandgap, facile synthesis, high monodispersity and solution processablity.[1-5] Advances in managing quantum dots' surface chemistry, as well as progress in device architecture, have recently led to certified AM1.5 solar power conversion efficiencies (PCEs)[6-9] of 9.9%.[1, 7, 10-14]

Colloidal quantum dots capped with suitable ligands can be redispersed in a range of solvents,[15-22] enabling fabrication ranging from layer-by-layer (LBL) spin-casting [23-25] to spray-coating,[26-27] inkjet printing,[28-29] and dip coating.[30-32] These multilayer approaches involve repeated quantum dot deposition, solid-state ligand exchanges, and rinse steps, resulting both in low quantum dot utilization and high solvent consumption.[33]

With the limitations of layer-by-layer methods in mind, researchers have recently focused on fabricating CQD solar cells based on pre-exchanged CQD inks. These can be directly deposited, simplifying the manufacturing, and using materials and solvents more efficiently.[33-35] Unfortunately, the highest-performing devices reporetd to date based on this approach have been limited to PCEs of 6%, considerably below the best layer-by-layer CQD devices.

Liganding CQDs using methylammonium iodide (MAI) was recently shown to offer the possibility of short-ligand-exchanged CQDs that could be directly deposited from a polar solvent.[20] Very recently, it was reported that PbS quantum dots and methylammonium lead triiodide perovskites ($MAPbI_3$) can exhibit coherence in their lattice fringes owing to their minimal lattice mismatch.[36]

Here we investigate the fabrication of solar cells that employ PbS colloidal quantum dots that, once formed into solid-state films, are passivated using a thin matrix of $MAPbI_3$. Inspired by previous investigations of CQD-embedded perovskite solids,[36] we prepared concentrated CQD

inks that were prepared to enable subsequent perovskite shelling once formed into films. We find that the films of perovskite-shelled CQDs exhibit a depletion region depth of ~120 nm, indicating a notably lower doping level than in the best prior CQD photovoltaic films. We fabricate CQD solar cells based on the directly-deposited composite active medium, and these reach PCEs of 8.95%, a 1.45x improvement over the previous champion CQD-ink-based device.[35]

PbS CQDs were synthesized and purified using an established hot-injection approach and anti-solvent method, respectively.[11] Solution ligand exchange was achieved by mixing the CQD octane solution (~20 mg/mL) and dimethylformamide (DMF) solution containing $MAPbI_3$ perovskite precursors (MAI and PbI_2, 0.3 mol/L). The $MAPbI_3$ ligand passivation renders CQDs soluble in DMF that can then be re-precipitated upon addition of toluene. This solvent/anti-solvent purification process was repeated twice to remove the residual oleic acid (OA), and the purified CQDs were finally redispersed in dry butylamine to yield a concentrated ink in a solvent with low boiling point (Figure 1a).

Compared to the absorption spectrum of OA-capped CQDs in solution, the $MAPbI_3$-passivated CQD films are redshifted from 870 nm to 940 nm (Figure 1b), comparable to conventional films solid-state exchanged with tetrabutylammonium iodide ligand. A 75 nm redshift was seen in photoluminescence spectra of $MAPbI_3$-capped dots in solution compared to their OA-capped counterparts (Figure 1c). We note that both the shift and broadening of the PL spectrum are smaller than in prior reports of CQDs passivated using MAI alone.[35] This suggests better surface coverage and less CQD aggregation when both PbI_2 and MAI were employed as ligands. The photoluminescent quantum yield of spin-cast $MAPbI_3$-capped CQD film is around 2%, which is comparable to the report values of inorganic shell passivated CQD films.[36-37] X-ray diffraction (XRD) of annealed films and powders are dominated by PbS signals (Figure 2d), i.e.

XRD does not resolve the perovskite crystal phase, a finding that we attribute to the perovskite's low concentration and the limits of XRD signal-to-background.

We therefore turned to TEM to investigate whether a thin perovskite shell/matrix was being formed. As seen in Figure 2a, a continuous solid matrix connects together the PbS quantum dots. Careful analysis with high resolution imaging (Figure 2b-c) indicates that the resultant lattice is coherent with that of nearby quantum dots. Scanning tunneling electron microscope (STEM) imaging provided additional information regarding the presence of perovskite: (Figure S2). the majority of CQDs examined showed lattice fringes spaced by 3.4 Å, and this corresponds to the {111} plane spacing for cubic PbS.[38] STEM also revealed another set of lattice fringes with d-spacing of 3.7 Å, consistent with the {022} plane spacing for $MAPbI_3$ crystals.[39]

XPS of the annealed $MAPbI_3$-CQD mixed materials showed appreciable nitrogen 1s (~402 eV), iodine 3d (~619 eV), and lead 4f (142.5 and 137.5 eV for $4f_{5/2}$ and $4f_{7/2}$, respectively), and the oxidation state of the N and I are closely aligned with those of pure $MAPbI_3$ perovskite crystals (Figures 2e).

CQD solar cells have recently been shown that leverage a stable n-type CQD solid combined with a p-type top layer.[22] We projected that the $MAPbI_3$ CQD layers would exhibit similar band positions to TBAI-passivated layers, and we therefore constructed devices following a similar architecture (Figure 3). Indium-doped tin oxide (ITO) coated glass was used as substrate, on top of which a layer of solution-processable ZnO nanoparticles was deposited by spin-casting. The concentrated butylamine solution of exchanged $MAPbI_3$-passivated CQD was directly spin-cast and formed a uniform mirror-like dark-brown film. This was further annealed at 70°C under inert atmosphere for 10 min to allow formation of perovskite in the manner documented in Figure 2. A layer consisting of oleic-acid-capped CQDs (original absorption peak at 870 nm) was then

deposited on top of the $MAPbI_3$-PbS main absorber and solid-state ligand-exchanged using EDT to form a p-type top layer.[13-14] The optimized thickness of $MAPbI_3$-PbS and EDT-PbS layers were 200 nm and 50 nm, respectively (Figure 3a).

We observed that annealing, with the goal of transforming the perovskite precursors into a thin crystalline matrix, was required to achieve the best device performance levels reported herein. Annealed and non-annealed performance under AM 1.5 solar illumination are reported in Figure 3b and Table S1. The J_{sc} and V_{oc} of annealed devices are ~21.9 mA/cm^2 and 0.61 V, over 10% and 22% higher than the parameters of the non-annealed sample, respectively. The improvement is also reflected in higher fill factor (FF) and reduced hysteresis, yielding a power conversion efficiency (PCE) of 8.5%. All device parameters are significantly higher than those from the best device treated using the previously-published MAI ligand exchange (Figure 3c).[35] We conclude that the inclusion of the coherently-lattice-matching passivating thin layer of $MAPbI_3$ perovskite limits CQD aggregation and thus achieves a better balance of V_{oc} and J_{sc}, yielding improved device performance.

Considering the band misalignment between $MAPbI_3$- and EDT-capped PbS layers, we further optimized the device by using an EDT treated layer incorporating slightly larger dots (absorption peak of purified OA-capped dots at 896 nm). The optimization led to an increase in FF to ~68% and the resultant PCE of 8.95%. This is 1.45x higher than the previous record of a CQD solar cell based on a directly-deposited solution-processed principal active layer. We found that the materials do change gradually under time, especially in the presence of light exposure (Figure S3),[40] leading to a decrease in J_{sc} over the course of characterization, a fact that accounts for the slightly lower overall external quantum efficiency than in TBAI-passivated devices (Figure 4b).[13-14]

We sought to elucidate the origins of improved performance relative to prior direct-deposit reports. We characterized the diffusion length (L_{diff}) and depletion width (W_D) in our solar cells for comparison to controls. L_{diff} was obtained by measuring the bias-dependent collection efficiency (see Methods) and fitting to a previously-reported analytical model.[41] We found L_{diff} to be of order 60 nm (Figure 4c). Given the thickness of the active layer in our devices (~200 nm) and the high fill-factor attained (68%), this suggests that drift is playing a significant role in charge collection. Indeed, capacitance-voltage spectroscopy (Figure 4d) reveals that perovskite-passivated dot films remain fully depleted at short-circuit conditions, with a depletion width of 120 nm at maximum power point conditions. The obtained carrier density of 4×10^{16} cm^{-3} suggests that the perovskite matrix passivation results in a more fully depleted CQD solid compared to prior passivation schemes such as those based on TBAI.[14] This is consistent with the highly intrinsic nature of perovskite active layers observed in perovskite photovoltaic studies.

In conclusion, the present study demonstrates the fabrication of perovskite-passivated CQD solids. Solution ligand exchange using perovskite precursors, followed by annealing to promote matrix crystallization, led to the formation of perovskite thin shells onto CQD surfaces. The addition of a larger-bandgap perovskite matrix created a more intrinsic CQD film exhibiting a deeper depletion region of 120 nm at working conditions, notably thicker than in prior solid-state-exchanged reports. Optimization of the device and its processing led to a PCE of 8.95%, a major advance over prior directly-deposited CQD devices. Since excellent surface passivation for improved open-circuit voltage is the most quantitatively significant opportunity for improved CQD solar cell performance, we believe that further effort is warranted in epitaxial matrix incorporation in CQD photovoltaic solids.

ASSOCIATED CONTENT

Supporting Information includes experimental details of PbS CQD synthesis, perovskite ligand exchange, device fabrication and characterization, as well as TEM images of OA- and MAI-capped PbS CQDs. The material also includes STEM images of perovskite-capped CQDs, time-dependent short circuit current measurements of $MAPbI_3$-shelled devices, and Table that shows performance parameters of CQD devices with different surface ligands and preparation processes. This material is available free of charge via the Internet at http://pubs.acs.org.

AUTHOR INFORMATION

Corresponding Author

*Address correspondence to ted.sargent@utoronto.ca.

Notes

Conflict of Interest: The authors declare no competing financial interest.

ACKNOWLEDGMENT

This publication is based in part on supported by Award KUS-11-009-21, from King Abdullah University of Science and Technology (KAUST), by the Ontario Research Fund - Research Excellence Program, by the Natural Sciences and Engineering Research Council (NSERC) of Canada, and by the International Cooperation of the Korea Institute of Energy Technology Evaluation and Planning (KETEP) grant funded by the Korea government Ministry of Knowledge Economy (2012T100100740). A.J. thanks NSERC for Undergraduate Student Research Award Funding. E.Y. acknowledges support from FAPESP-BEPE fellowship (2014/18327-9). The authors thank E. Palmiano, L. Levina, R. Wolowiec, and D. Kopilovic for helpful discussions.

REFERENCES

1. McDonald, S. A.; Konstantatos, G.; Zhang, S.; Cyr, P. W.; Klem, E. J. D.; Levina, L.; Sargent, E. H., *Nat. Mater.* **2005,** *4* 138-142.

2. Kamat, P. V., *J. Phys. Chem. C.* **2008,** *112* 18737-18753.

3. Luther, J. M.; Law, M.; Beard, M. C.; Song, Q.; Reese, M. O.; Ellingson, R. J.; Nozik, A. J., *Nano Lett.* **2008,** *8* 3488-3492.

4. Nozik, A. J.; Beard, M. C.; Luther, J. M.; Law, M.; Ellingson, R. J.; Johnson, J. C., *Chem. Rev.* **2010,** *110* 6873-6890.

5. Carey, G. H.; Abdelhady, A. L.; Ning, Z.; Thon, S. M.; Bakr, O. M.; Sargent, E. H., *Chem. Rev.* **2015**.

6. Murray, C. B.; Norris, D. J.; Bawendi, M. G., *J. Am. Chem. Soc.* **1993,** *115* 8706-8715.

7. Tang, J.; Kemp, K. W.; Hoogland, S.; Jeong, K. S.; Liu, H.; Levina, L.; Furukawa, M.; Wang, X.; Debnath, R.; Cha, D.; Chou, K. W.; Fischer, A.; Amassian, A.; Asbury, J. B.; Sargent, E. H., *Nat. Mater.* **2011,** *10* 765-771.

8. Kramer, I. J.; Sargent, E. H., *Chem. Rev.* **2014,** *114* 863-882.

9. Brown, P. R.; Kim, D.; Lunt, R. R.; Zhao, N.; Bawendi, M. G.; Grossman, J. C.; Bulović, V., *ACS Nano* **2014,** *8* 5863-5872.

10. Luther, J. M.; Gao, J.; Lloyd, M. T.; Semonin, O. E.; Beard, M. C.; Nozik, A. J., *Adv. Mater.* **2010,** *22* 3704-3707.

11. Ip, A. H.; Thon, S. M.; Hoogland, S.; Voznyy, O.; Zhitomirsky, D.; Debnath, R.; Levina, L.; Rollny, L. R.; Carey, G. H.; Fischer, A.; Kemp, K. W.; Kramer, I. J.; Ning, Z.; Labelle, A. J.; Chou, K. W.; Amassian, A.; Sargent, E. H., *Nat. Nanotech.* **2012,** *7* 577-582.

12. Semonin, O. E.; Luther, J. M.; Choi, S.; Chen, H.-Y.; Gao, J.; Nozik, A. J.; Beard, M. C., *Science* **2011,** *334* 1530-1533.

13. Chuang, C.-H. M.; Brown, P. R.; Bulović, V.; Bawendi, M. G., *Nat. Mater.* **2014,** *13* 796-801.

14. Lan, X.; Voznyy, O.; Kiani, A.; García de Arquer, F. P.; Abbas, A. S.; Kim, G.-H.; Liu, M.; Yang, Z.; Walters, G.; Xu, J.; Yuan, M.; Ning, Z.; Fan, F.; Kanjanaboos, P.; Kramer, I.; Zhitomirsky, D.; Lee, P.; Perelgut, A.; Hoogland, S.; Sargent, E. H., *Adv. Mater.* **2015,** *In revision*.

15. Huynh, W. U.; Dittmer, J. J.; Alivisatos, A. P., *Science* **2002,** *295* 2425-2427.

16. Konstantatos, G.; Howard, I.; Fischer, A.; Hoogland, S.; Clifford, J.; Klem, E.; Levina, L.; Sargent, E. H., *Nature* **2006,** *442* 180-183.

17. Kovalenko, M. V.; Scheele, M.; Talapin, D. V., *Science* **2009,** *324* 1417-1420.

18. Ning, Z.; Ren, Y.; Hoogland, S.; Voznyy, O.; Levina, L.; Stadler, P.; Lan, X.; Zhitomirsky, D.; Sargent, E. H., *Adv. Mater.* **2012,** *24* 6295-6299.

19. Jang, J.; Liu, W.; Son, J. S.; Talapin, D. V., *Nano Lett.* **2014,** *14* 653-662.

20. Dirin, D. N.; Dreyfuss, S.; Bodnarchuk, M. I.; Nedelcu, G.; Papagiorgis, P.; Itskos, G.; Kovalenko, M. V., *J. Am. Chem. Soc.* **2014,** *136* 6550-6553.

21. Zhang, H.; Jang, J.; Liu, W.; Talapin, D. V., *ACS Nano* **2014,** *8* 7359-7369.

22. Ning, Z.; Voznyy, O.; Pan, J.; Hoogland, S.; Adinolfi, V.; Xu, J.; Li, M.; Kirmani, A. R.; Sun, J.-P.; Minor, J.; Kemp, K. W.; Dong, H.; Rollny, L.; Labelle, A.; Carey, G.; Sutherland, B.; Hill, I.; Amassian, A.; Liu, H.; Tang, J.; Bakr, O. M.; Sargent, E. H., *Nat. Mater.* **2014,** *13* 822-828.

23. Cassagneau, T.; Mallouk, T. E.; Fendler, J. H., *J. Am. Chem. Soc.* **1998,** *120* 7848-7859.

24. Shimomura, M.; Sawadaishi, T., *Current Opinion in Colloid & Interface Science* **2001,** *6* 11-16.

25. Fu, Y.; Xu, H.; Bai, S.; Qiu, D.; Sun, J.; Wang, Z.; Zhang, X., *Macromolecular Rapid Communications* **2002,** *23* 256-259.

26. Kramer, I. J.; Minor, J. C.; Moreno-Bautista, G.; Rollny, L.; Kanjanaboos, P.; Kopilovic, D.; Thon, S. M.; Carey, G. H.; Chou, K. W.; Zhitomirsky, D.; Amassian, A.; Sargent, E. H., *Adv. Mater.* **2015,** *27* 116-121.

27. Kramer, I. J.; Moreno-Bautista, G.; Minor, J. C.; Kopilovic, D.; Sargent, E. H., *Appl. Phys. Lett.* **2014,** *105* 163902.

28. Guo, Q.; Kim, S. J.; Kar, M.; Shafarman, W. N.; Birkmire, R. W.; Stach, E. A.; Agrawal, R.; Hillhouse, H. W., *Nano Lett.* **2008,** *8* 2982-2987.

29. Wood, V.; Panzer, M. J.; Chen, J.; Bradley, M. S.; Halpert, J. E.; Bawendi, M. G.; Bulović, V., *Adv. Mater.* **2009,** *21* 2151-2155.

30. Yang, C.-C.; Y. Josefowicz, J.; Alexandru, L., *Thin Solid Films* **1980,** *74* 117-127.

31. Labelle, A. J.; Thon, S. M.; Masala, S.; Adachi, M. M.; Dong, H.; Farahani, M.; Ip, A. H.; Fratalocchi, A.; Sargent, E. H., *Nano Lett.* **2015,** *15* 1101-1108.

32. Labelle, A. J.; Thon, S. M.; Kim, J. Y.; Lan, X.; Zhitomirsky, D.; Kemp, K. W.; Sargent, E. H., *ACS Nano* **2015,** *9* 5447-5453.

33. Fischer, A.; Rollny, L.; Pan, J.; Carey, G. H.; Thon, S. M.; Hoogland, S.; Voznyy, O.; Zhitomirsky, D.; Kim, J. Y.; Bakr, O. M.; Sargent, E. H., *Adv. Mater.* **2013,** *25* 5742-5749.

34. Giansante, C.; Carbone, L.; Giannini, C.; Altamura, D.; Ameer, Z.; Maruccio, G.; Loiudice, A.; Belviso, M. R.; Cozzoli, P. D.; Rizzo, A.; Gigli, G., *J. Phys. Chem. C.* **2013,** *117* 13305-13317.

35. Ning, Z.; Dong, H.; Zhang, Q.; Voznyy, O.; Sargent, E. H., *ACS Nano* **2014,** *8* 10321-10327.

36. Ning, Z.; Gong, X.; Comin, R.; Walters, G.; Fan, F.; Voznyy, O.; Yassitepe, E.; Buin, A.; Hoogland, S.; Sargent, E. H., *Nature* **2015,** *523* 324-328.

37. Moroz, P.; Liyanage, G.; Kholmicheva, N. N.; Yakunin, S.; Rijal, U.; Uprety, P.; Bastola, E.; Mellott, B.; Subedi, K.; Sun, L.; Kovalenko, M. V.; Zamkov, M., *Chem. Mater.* **2014,** *26* 4256-4264.

38. Lingley, Z.; Mahalingam, K.; Lu, S.; Brown, G.; Madhukar, A., *Nano Res.* **2014,** *7* 219-227.

39. Stoumpos, C. C.; Malliakas, C. D.; Kanatzidis, M. G., *Inorganic Chemistry* **2013,** *52* 9019-9038.

40. Hoke, E. T.; Slotcavage, D. J.; Dohner, E. R.; Bowring, A. R.; Karunadasa, H. I.; McGehee, M. D., *Chemical Science* **2015,** *6* 613-617.

41. Kemp, K. W.; Wong, C. T. O.; Hoogland, S. H.; Sargent, E. H., *Appl. Phys. Lett.* **2013,** *103* 211101.

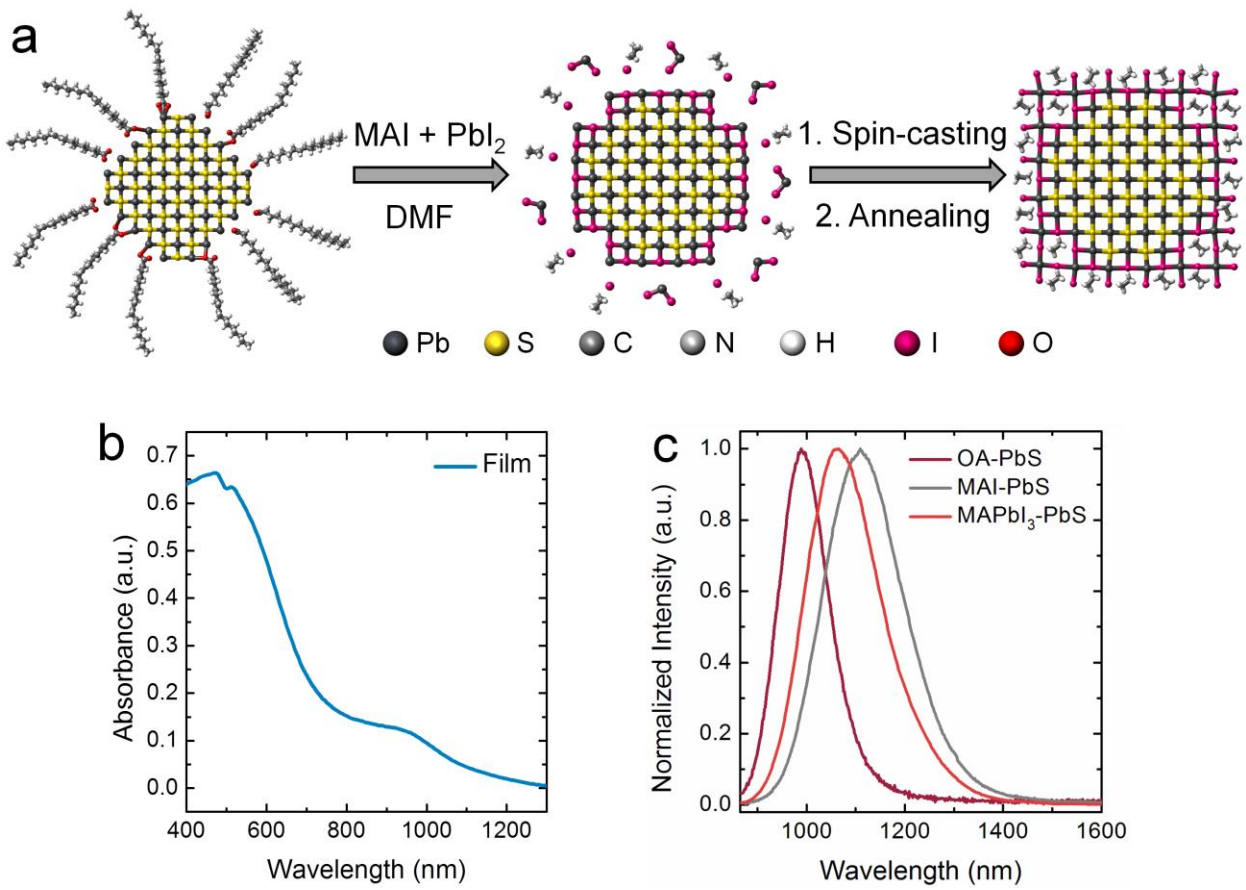

Figure 1. PbS CQDs passivated using ligands that supply the chemical precursors to lead methylammonium perovskites: optical properties and processing. (a) Schematic of solution ligand exchange with perovskite precursors and corresponding CQD film preparation. (b) Absorption spectrum of $MAPbI_3$-capped PbS CQD film showing CQD absorption peak at 940 nm. (c) Solution photoluminescence (PL) spectra of PbS CQDs passivated using various ligands. The reduced peak shift and peak broadening after exchange using $MAPbI_3$ precursors suggests a lesser degree of aggregation than in the MAI case.

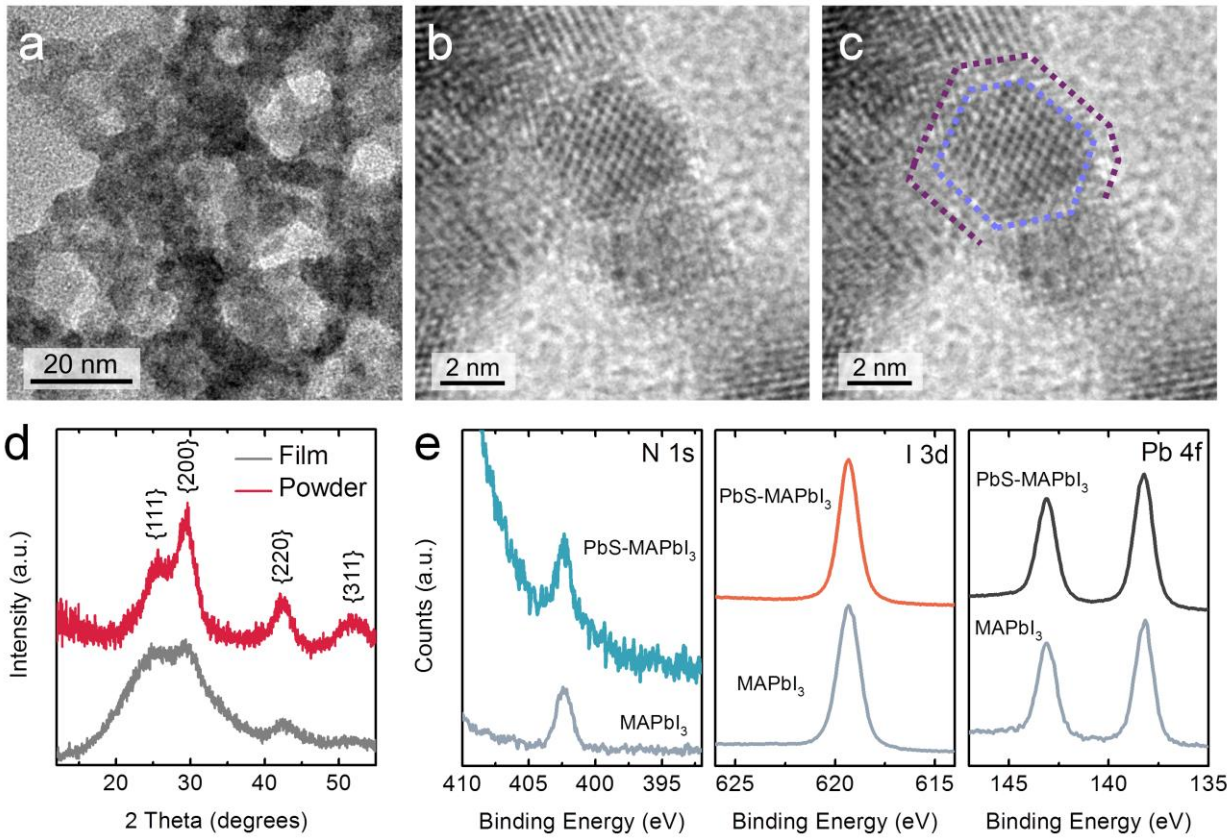

Figure 2. Characterization of perovskite-capped CQD films. (a) TEM images of $MAPbI_3$-capped CQD solid. (b) High-resolution TEM image showing the core-shell structure. (c) TEM image (same as in (b), but with dotted lines to guide the eye to evidence of a thin perovskite shell). (d) XRD patterns of $MAPbI_3$-capped CQD solid indicating the presence of PbS CQDs. (e) XPS results of nitrogen 1s, iodine 3d, and lead 4f regions of $MAPbI_3$-capped CQD film indicate the incorporation of $MAPbI_3$.

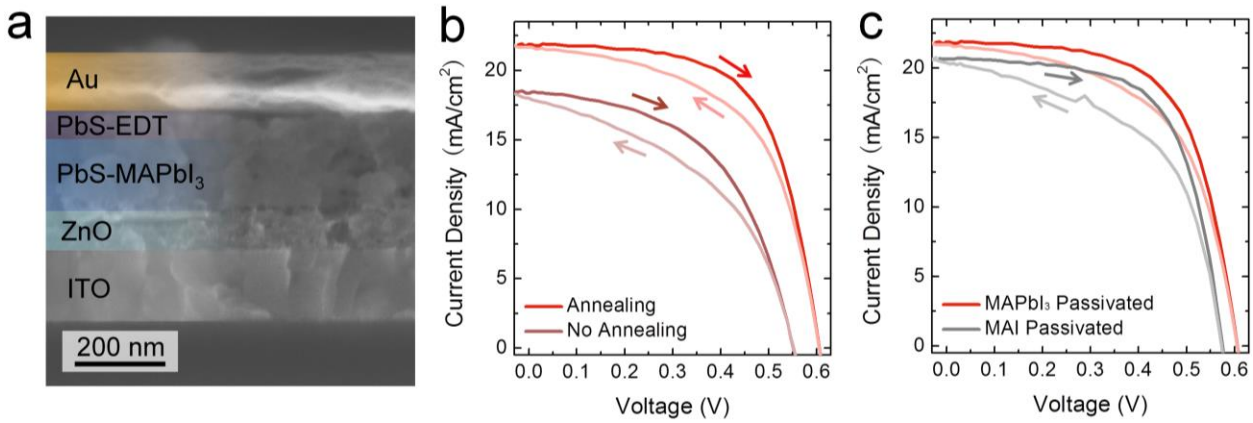

Figure 3. Photovoltaic device architecture and performance. (a) Cross-sectional SEM image with labels to indicate each component. (b) Current-voltage (*J-V*) characteristics under simulated AM 1.5 illumination for $MAPbI_3$-passivated devices with and without annealing. Lighter curves showing the *J-V* properties under reverse scanning indicate the reduction of hysteresis following annealing. (c) Comparison of *J-V* characteristics under simulated AM 1.5 illumination between $MAPbI_3$- and MAI-passivated devices.

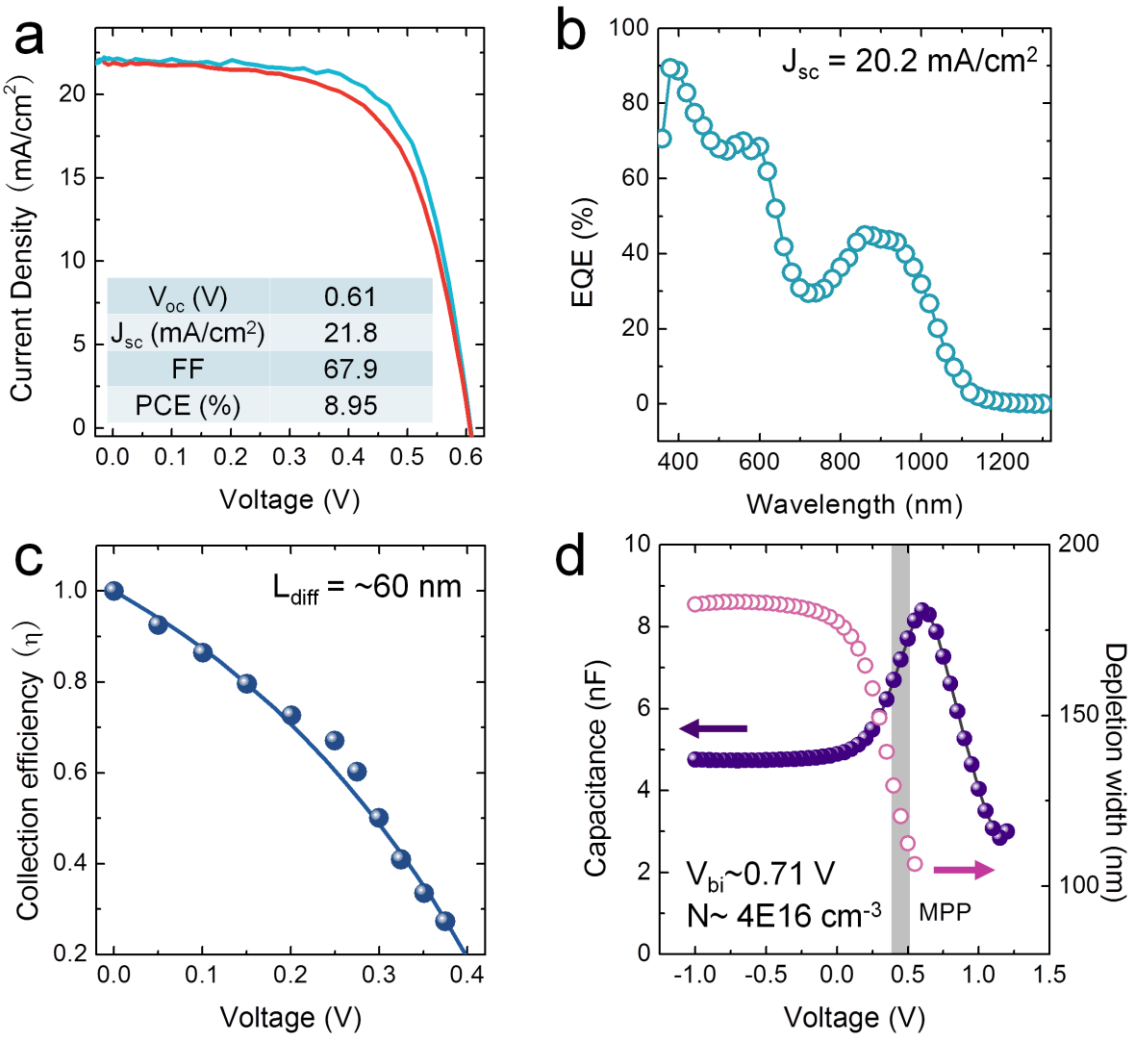

Figure 4. Performance of perovskite-shelled CQD photovoltaic devices. (a) *J-V* characteristics under simulated AM 1.5 illumination for $MAPbI_3$-shelled dot devices that employ smaller dots (blue) and larger dots (red) in the realization of the top EDT-solid-state-treated CQD layer. (b) EQE spectrum of a champion graded $MAPbI_3$-passivated device. (c) A diffusion length (L_{diff}) of 60 nm is obtained by fitting the collection efficiency with the aid of an analytical model (see methods). (d) Depletion width (W_D) as calculated from capacitance-voltage spectroscopy measurements. Devices remain fully depleted at short-circuit conditions. At maximum power point conditions (MPP), a W_D of 120 nm is obtained, consistent with the importance of drift in achieving efficient charge collection in these films. The perovskite shelling leads to more depleted films (4E16 cm^{-3}) compared to previously-reported passivation strategies.

TABLE OF CONTENTS GRAPHIC